Computational Materials Science 171 (2020) 109223

Contents lists available at ScienceDirect

Computational Materials Science

journal homepage: www.elsevier.com/locate/commatsci

Mechanism of surface nanostructure changing wettability: A molecular dynamics simulation

Lei Chen*, Shan-You Wang, Xing Xiang, Wen-Quan Tao

Key Laboratory of Thermo-Fluid Science and Engineering, Ministry of Education, School of Energy & Power Engineering, Xi'an Jiaotong University, Xi'an, Shaanxi 710049, People's Republic of China

ARTICLE INFO

Keywords:
Molecular dynamics simulation
Nanostructured surface
Wenzel
Cassie
Equivalent virtual surface

ABSTRACT

Molecular dynamics simulation is performed to simulate the wetting behavior of nano water droplets on flat and pillar surfaces. The result shows that the contact angle of the water droplet on the flat surface becomes smaller with the increase of the surface characteristic energy parameter ε. At the same energy parameter ε, the hydrophobicity is enhanced on the pillar surface compared to the flat surface. For nanostructured surfaces with different geometrical features, the sparser the surface pillars, the larger the contact angle. What's more, we propose an equivalent potential well method, which can effectively reveal the mechanism of nanostructures changing surface wettability. The deeper the equivalent potential well, the smaller the contact angle.

1. Introduction

Wettability of solid surface is an important feature which matters the ability of a solid surface to adsorb droplets. Superhydrophobic surfaces play a role in many applications, such as the self-cleaning effect of lotus leaves [1], the leg hair of striders [2], the anti-icing surfaces [3], and the enhanced phase change heat transfer surfaces [4]. With the development of microfluidic systems, the emergence of new materials, and the increasing interest in micro-level research, nanowetting is valued by more and more researchers.

Molecular dynamics simulation is an effective way to investigate the nanoflow and interfacial properties. The wettability of the solid surface depends mainly on the material and the topography of the solid surface, in addition, the presence of external field could also affect the wettability of solid surface. Considering the contact angle of water droplet on different materials or different conditions, lots of researches have been carried out. Werder et al. [5] investigated the wettability of carbon nanotubes and reported that carbon nanotubes were hydrophobic at room temperature. Janne et al. [6] studied the wettability of polyethylene surface, they constructed crystalline polyethylene surface and amorphous polyethylene surface respectively and proposed that the contact angle on polymer surface was concerned with the crystallinity. Ohler et al. [7] found that there existed an ice-like water film on the surface of titanium dioxide because of the special structure of the crystal. Dutta et al. [8] reported the wetting transition temperature of graphite and boron-nitride. On similar graphene surface, Burt et al. [9] researched the spreading of ionic-liquid droplets. On graphene-coated copper surfaces, Chinh et al. [10] found that the number of graphene layers had small effect on the contact angle. Chen et al. [11,12] did some work of water contact angle on quartz surfaces under supercritical carbon dioxide sequestration conditions. Zhang et al. [13] focused on the contact angle on soil minerals. In these studies, researchers only focused on the wettability of certain material in certain conditions, and the research objects were almost flat surfaces, but the surface structure matters the wettability actually [14].

Frequently, the contact angle on ideal flat surface is considered as the intrinsic contact angle, while abnormal wetting behavior associated with surface nanostructures is referred to as the apparent contact angle. There are two classic models for the wetting behavior of rough surfaces, Wenzel model [15] and Cassie model [16]. Chen et al. [17] found that the equilibrium wetting states could be classified into four categories: the Wenzel, the metastable Cassie, the globally steady Cassie, and the Cross state. Niu et al. [18] reported that the droplet in either the Wenzel state or the Cassie state depended on the height of the pillars and the pillar surface fraction. On the similar pillar surface, Chen et al. [19] changed the material into polytetrafluorethylene and simulations showed that the final wetting state depended on the initial geometry and cross contact was a metastable wetting state. Contact angle is usually affected by external fields. The influence of external electric field on contact angle is studied the most [20–22]. Daub et al. [20] demonstrated that the water contact angle was significantly sensitive to the applied electric field, polarity, and direction relative to the liquid/

* Corresponding author.
E-mail address: chenlei@mail.xjtu.edu.cn (L. Chen).

https://doi.org/10.1016/j.commatsci.2019.109223
Received 27 April 2019; Received in revised form 24 August 2019; Accepted 24 August 2019
Available online 05 September 2019
0927-0256/

solid interface. Under external electric field, Daub et al. [21] also investigated the electrowetting properties of salty nanodroplets and they found that the dependence of the contact angle on the field strength varied nonmonotonically with salt concentration. Recently, Song et al. [22] reported the wetting characteristics of nanometer-scale water droplets on a rough silicon solid substrate under vertical electric field. In addition to the electric field, there are other fields that have an effect on the contact angle. Bo et al. [23] described the change of surface tension of droplets with temperature and caused the contact angle to change with temperature, and tried to give a quantitative relationship. Fei et al. [24] applied molecular dynamics simulation to predict the nanofluidic contact angle offset by an AFM. In addition, many papers have described the dynamic characteristics of the contact angle [25,26]. And Blake et al. [27] did great work to combine molecular dynamics simulation and molecular-kinetic theory, this work makes the understanding of dynamic wetting deeper. Almost all above studies explain the change of contact angle by certain cases. So, in this paper, we will study the influences of surface nanostructures on wettability by molecular dynamics simulation, and propose the equivalent virtual surface analysis to judge the change of wettability of nanostructured surface.

2. Simulation methods and details

All classical molecular dynamics simulations in this study were performed with LAMMPS [28]. Interactions between molecules are usually described as a potential function, which is related to the nature of the molecular force. For the short-range van der Waals force, the Lennard-Jones potential function was employed in this study, which is abbreviated as L-J 12–6 potential. The most common expression of L-J 12–6 potential is:

$$U_{non-bond}(r) = 4\varepsilon\left[\left(\frac{\sigma}{r}\right)^{12} - \left(\frac{\sigma}{r}\right)^{6}\right] \tag{1}$$

For the long-range Coulombic force, electric potential was considered as:

$$U_e(r) = \frac{q_i q_j}{Dr} \tag{2}$$

Parameters used in Eqs. (1) and (2) are specified for certain atom type and can be fitted to reproduce experimental data or accurate quantum chemistry calculations. And σ means the finite distance at which the inter-particle potential is zero, r is the distance between particles, ε is the depth of potential well, q means the atomic charge, D represents the dielectric constant. Water was modeled using SPC/E water model [29], a three-site rigid model with charge at each point. To study the contact angle of sessile nanodroplet on a solid surface, a solid wall was placed at the bottom of the simulation box. Former research confirmed that the modeling of frozen surface resulted in neglectable difference in the contact angle as compared with that obtained using a flexible solid potential, especially for metal solid surface. Therefore, in the present study, the interactions between solid atoms were neglected. And the interactions between solid atoms and water molecules were considered as L-J 12–6 potential. Besides, the van der Waals interactions between different atomic species were calculated using Lentz-Bertholet mixing rule, thatrule, which is performing arithmetic mean for distance parameter and geometric mean for energy parameter. Exact parameters [30] for employed force field are presented in Table 1.

In carrying out the simulation of contact angle of water droplet on an ideal solid surface, the size of the simulation box was set as $216.89 \times 28.92 \times 162.22\ \text{Å}^3$. The solid surface was set to consist of layers of atoms arranged as an FCC lattice with its ⟨0 0 1⟩ surface in contact with droplet. The solid wall was taken to be copper with a lattice constant of 3.615 Å. Then, 2856 water molecules were placed on the surface and were arranged as FCC structure initially, as illustrated in Fig. 1. Periodic boundary conditions were applied along x and y directions, meanwhile mirror boundary condition was used in the z direction.

Table 1
Force field parameters.

Interaction pair	ε [kcal/mol]	σ [Å]	q [e]
O_{water}	0.1554	3.166	−0.8476
H_{water}	0	0	0.4238
Cu	0.2379	2.34	–
Cu- O_{water}	0.1923	2.753	–
Cu- H_{water}	0	0	–

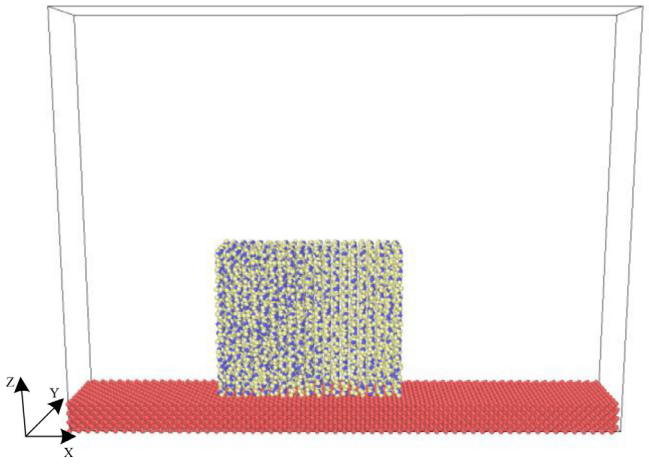

Fig. 1. Initial configuration of the simulated system, in which the red particles are solid atoms, purple ones are oxygen atoms, and yellow ones are hydrogen atoms.

The simulations were carried out in an NVT ensemble (fixed number of particles, volume, and temperature) at 300 K. Equations of motion was integrated numerically with a time step of 1 fs. The Nose-Hoover thermostat was used for temperature coupling with relaxation timesteps of 100. Electrostatic and van der Waals interactions were truncated with a 12 Å cutoff. And PPPM method was used to minimize the errors in long-range electrostatic interactions. The SHAKE algorithm [31] was performed to keep the water molecules as rigid bodies. Each system was equilibrated for 300 ps and typically ran additional 500 ps for sampling.

The systems can be regarded as quasi-three-dimensional systems because the periodic boundary in y direction. Therefore, to determine the contact angle of droplet on solid surface, the simulation domain was divided into two-dimensional chunks perpendicular to x-z plane. In order to draw a density contour, the density of water was calculated in each chunk whose size was $2 \times 2\ \text{Å}^2$.

3. Results and discussion

3.1. Determination of contact angle

Molecular dynamics simulations were carried out to study the contact angle of a nanodroplet on a solid surface. The dependence of contact angle on the thickness of solid surface, number of liquid molecules and L-J cutoff was considered according to previous studies. What's more, the adoption of quasi-three-dimensional simulation system has the advantage [32] to reduce the scale effect by eliminating the three-phase line tension. Besides, the contribution of gravity can be neglected in nanoscale.

As mentioned above, contact angle was measured from the density contour of droplet. For this purpose, density contour should be drawn from the time-average density of each chunks, using triangulation-based natural neighbor interpolation. In this study, the contact angle of water droplet on copper ⟨0 0 1⟩ surface was first investigated to ensure

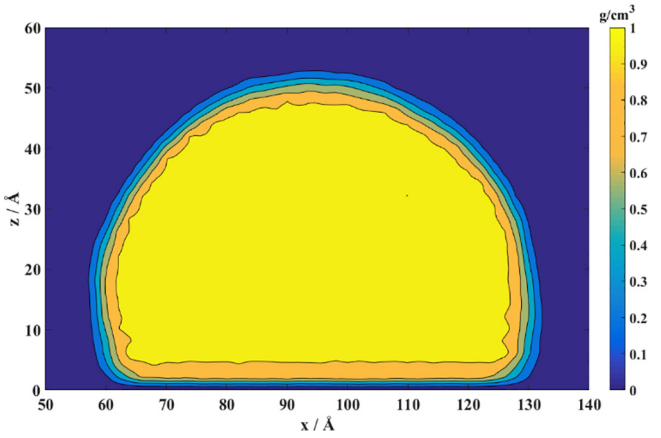

Fig. 2. Density contour of water droplet on copper surface.

the reliability and accuracy of molecular dynamics simulations in this study. A three layers copper crystal were built as the solid surface. Fig. 2 shows the time-average density profile of water droplet on copper surface. It can be observed that the shape of a water droplet may approximate a circle from the density contour. And there exists obvious transition layer at the liquid-vapor interface. It is also interesting to mention that there exists a remarkable isolated layer at the bottom of the water droplet, which is concerned with calculating the contact angle. The contour curve with density of 0.5 g/cm^3 is regarded as the liquid-vapor boundary. Assuming the water droplet to be perfectly rounded, the mathematical equation of circles could be expressed as:

$$(x - a)^2 + (z - b)^2 = R^2 \tag{3}$$

In Eq. (3), a and b are the x and z coordinates at the center of the circle, and R is the radius of the circle. Through least-square fitting process along liquid-vapor boundary, the values of a, b and R could be determined. Fig. 3 illustrates the determination of the contact angle of copper surface. The circles represent the coordinates along the water droplet boundary (liquid-vapor boundary), and the solid curve represents the fitting circle. The contact angle could be calculated using Eq. (4), where z_{sub} means the thickness of isolated layer at the bottom of the water droplet. Finally, the contact angle of water droplet on copper surface is 109°. Experimental measurement of contact angle of water droplet on the smooth copper surface is 102° [33]. Two factors may cause the difference between molecular dynamics simulation result and experiment measurement, on the one hand gravity should not be neglected if the macroscale droplet is large enough, on the other hand the actual surface used in experiment is not identical to the ideal surface

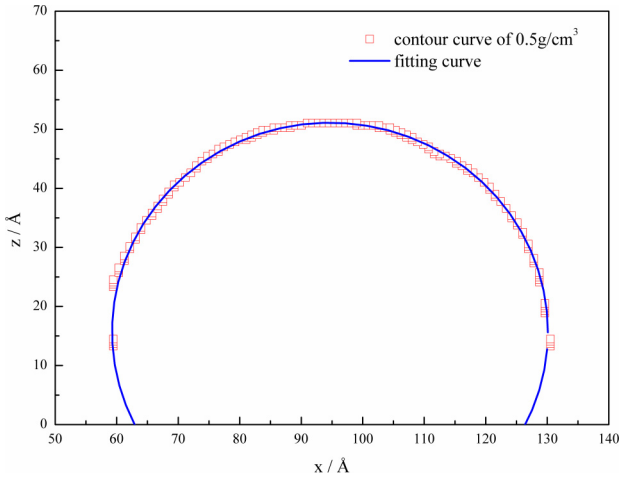

Fig. 3. Determination of contact angle.

investigated in this study. However, we can still consider the result of molecular dynamics simulation to be reliable because the error between simulation and experiment is very small.

$$\theta = arcsin\left(\frac{b - z_{sub}}{R}\right) + 90^o \tag{4}$$

3.2. Effect of surface characteristic energy

The properties of the solid surface effect the contact angle of water droplet on the surface the most, especially the surface characteristic energy in L-J potential. To study the wetting behavior of droplet on the ideal surface with different energy parameters, four solid surfaces with same lattice constant but different characteristic energies (ε_{solid} = 0.2379 kcal/mol for copper surface, ε_{solid1} = 0.4 kcal/mol, ε_{solid2} = 0.6 kcal/mol, ε_{solid2} = 0.8 kcal/mol) were built. Figs. 2–6 show the results of the four cases. From the density contours, it can be observed that the isolated layer at the bottom of the droplet gradually becomes an adsorption layer. For the surface with higher characteristic energy, water molecules attach strongly with the surface particles, so it is more likely to form an adsorption layer. On the other hand, water molecules are not friendly with a surface with low characteristic energy but combine with each other, and this makes it easier to form isolated layer. The contact angles obtained from the circle fitting curves are 110°, 95.3°, 75.9°, 62.3° for ε_{solid} = 0.2379 kcal/mol ε_{solid1} = 0.4 kcal/mol ε_{solid2} = 0.6 kcal/mol, ε_{solid2} = 0.8 kcal/mol, respectively. Accordingly, the contact angles can be considered as a function of the characteristic energies of solid wall, as illustrated in Fig. 7. As expected, increasing the characteristic energy of solid wall diminishes the contact angle. The conclusion can be drawn as follow: small characteristic energy represents weak interaction between solid particle and water which results in large contact angle, in contrast, large characteristic energy represents strong interaction and lead to small contact angle. That is the weak interaction means hydrophobic and the strong interaction means hydrophilic, and in the case of ideal flat surface this conclusion is applicable.

3.3. Effect of nanostructure

Experiments have shown that the surface structure can alter the wetting behavior. In the present study, this phenomenon will be discussed from the perspective of molecular dynamics simulation. To this end, water molecules located on the pillar surfaces were modeled. For the rough surfaces, pillars were placed on the flat surface. The thickness of the flat substrate is 10.845 Å equivalent to three times of lattice constant, and the height of the pillars is also 10.845 Å. Several pillars are evenly distributed on the flat substrate. The initial configuration is shown in Fig. 8. Here, P is defined as a geometric feature parameter to describe the roughness of the pillar surface which is the ratio of the pillar geometric projected area to the smooth surface. And the P value of the pillar surface shown in Fig. 8 is 0.4.

Figs. 9–12 show the time-average density contours for all simulated rough surfaces with different characteristic energies (ε_{solid} = 0.2379 kcal/mol, ε_{solid1} = 0.4 kcal/mol ε_{solid2} = 0.6 kcal/mol, ε_{solid2} = 0.8 kcal/mol). From the density contours, it can be observed that the wetting states on the surfaces with the same nanostructure but different characteristic energies are different. With the characteristic energy of 0.2379 kcal/mol, the contact angle of water droplet on flat surface is 110°, therefore the surface is intrinsically hydrophobic. For this reason, the interaction between pillar atoms and water molecules is weak and water molecules are not likely to penetrate into the gaps which results in Cassie wetting state. As the characteristic energy increasing, the transition from Cassie state to Wenzel state occurs. For surface with the characteristic energy of 0.4 kcal/mol, a mixed wetting behavior can be seen where the water molecules are not above the pillars totally, nor does the water molecules fill the gaps between pillars

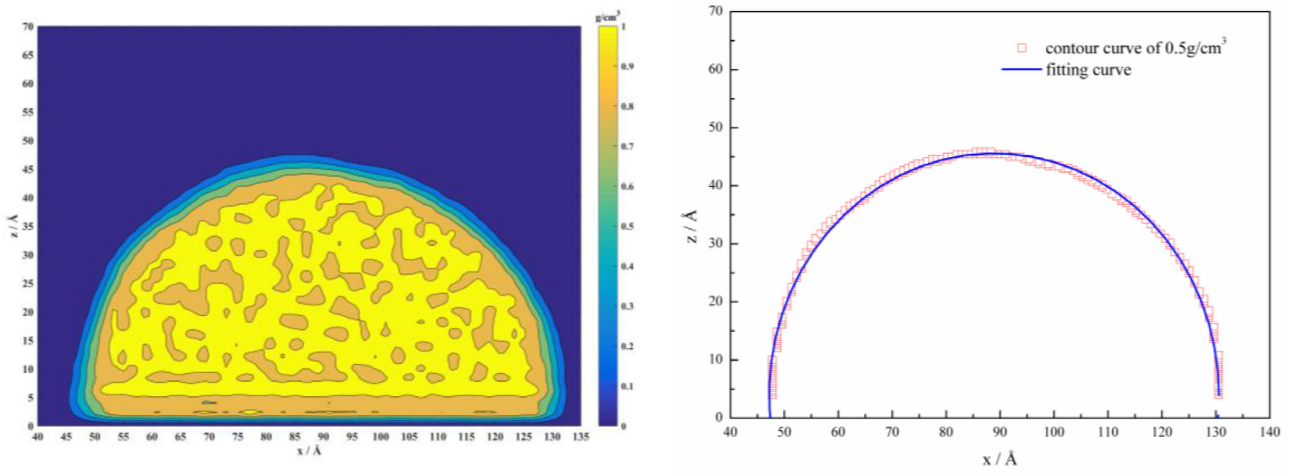

Fig. 4. Results for ε_{solid1} = 0.4 kcal/mol.

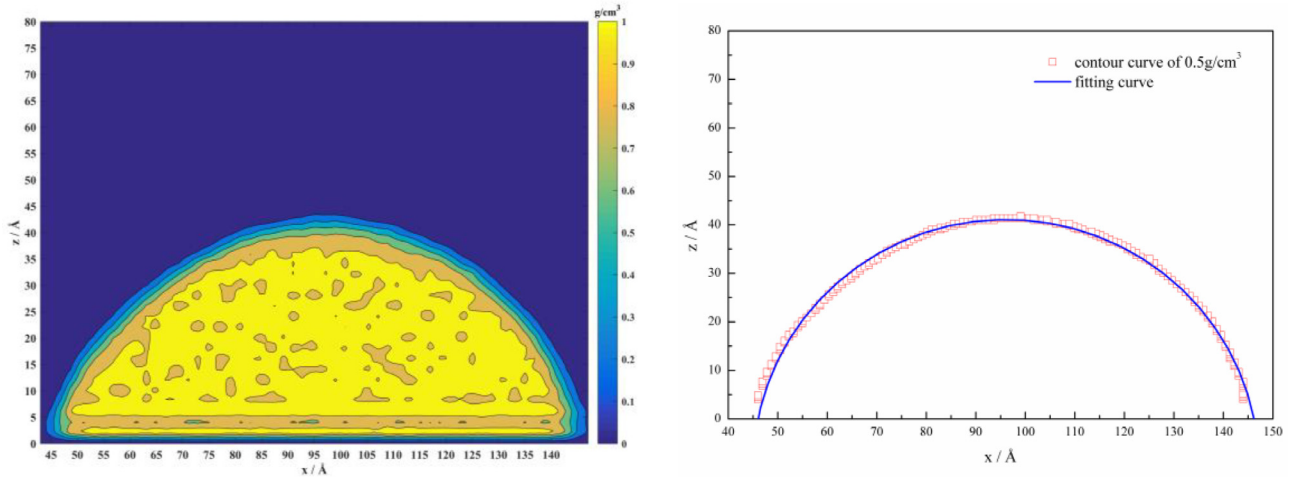

Fig. 5. Results for ε_{solid2} = 0.6 kcal/mol.

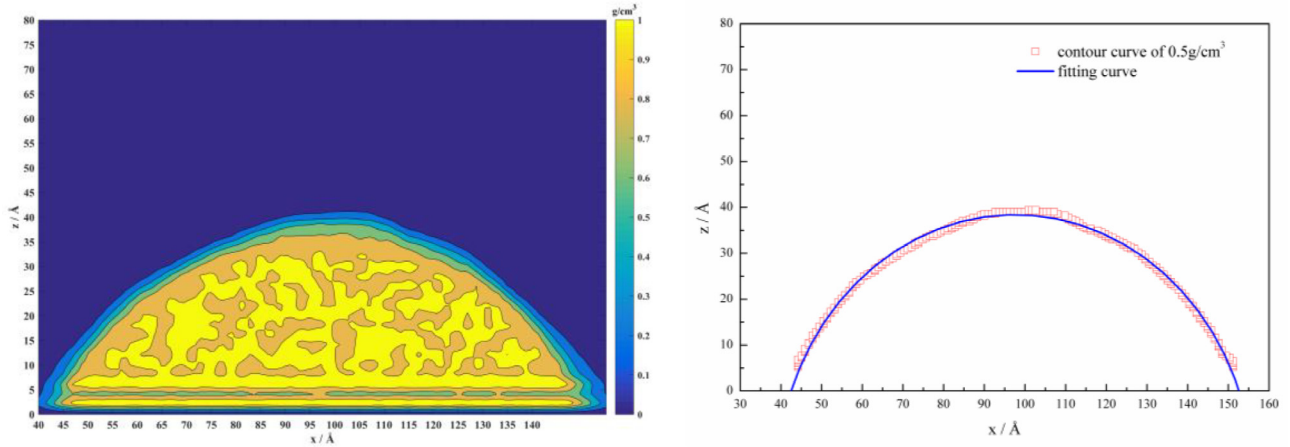

Fig. 6. Results for ε_{solid2} = 0.8 kcal/mol.

fully. The wetting behavior becomes Wenzel state when the characteristic energy of the solid particle reaches 0.6 kcal/mol and 0.8 kcal/mol. The conclusion can be drawn that Cassie state will happen when the surface characteristic energy is weak and wetting transition may occur when the surface characteristic energy becomes lager.

Fig. 13 shows the static contact angle varies with the characteristic energy of the solid particle. The contact angle of water droplet on pillar surface will decrease with the increasing characteristic energy. And this conclusion is consistent with it of water droplet on flat surface.

An interesting thing attracts notice when we compare the contact angles of smooth surfaces with those of rough surfaces. When the characteristic energy of solid particle is 0.2379 kcal/mol and 0.4 kcal/mol respectively, the intrinsic contact angles on smooth surface are lager than 90°, that means the surface with those characteristic energies

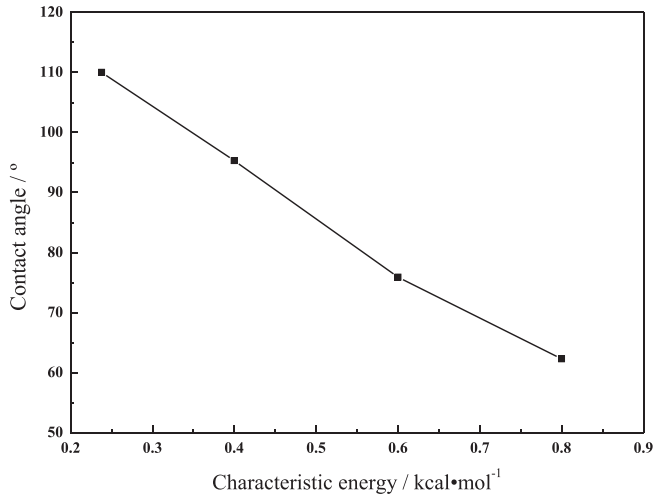

Fig. 7. Relationship between contact angle and characteristic energy, on the flat surface.

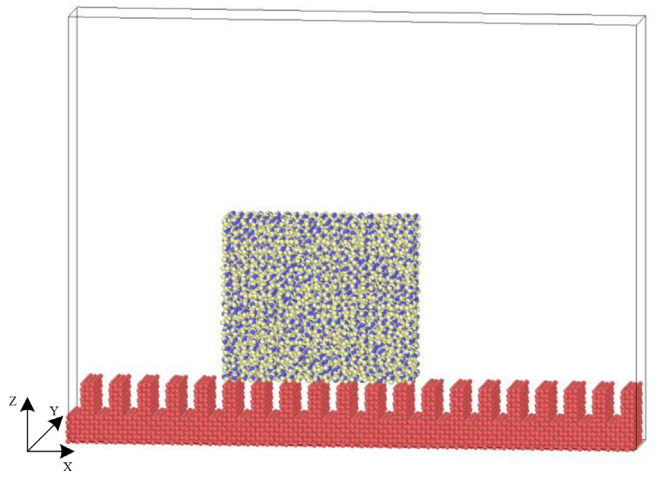

Fig. 8. Initial configuration of water droplet on pillar surface.

is intrinsically hydrophobic. And the intrinsically hydrophobic rough surface is more likely to form Cassie wetting state. In the Cassie model, water molecules could not fill the gaps on the pillar surface, and the relationship between apparent contact angle on rough surface and intrinsic contact angle can be written as:

$$cos\theta_{\text{apparent}} = P(cos\theta_{\text{intrinsic}} + 1) - 1 \quad (5)$$

For the rough surface with characteristic energy of 0.2379 kcal/mol, the intrinsic contact angle is 110°, P is 0.4, so the apparent contact angle calculated by Eq. (5) is 137.46°. Compared with the result from molecular dynamics simulation, 135.15°, the relative error is 1.71%. For the rough surface with characteristic energy of 0.4 kcal/mol, the intrinsic contact angle is 95.3°, and the calculated apparent contact angle is 129.56° which is consistent with the simulation result, 122.02°. Accordingly, for the intrinsic hydrophobic surface, the results of molecular dynamics simulation are consistent with Cassie model. As for the rough surfaces whose characteristic energies are 0.6 kcal/mol and 0.8 kcal/mol respectively, although the wetting behaviors are Wenzel state, they do not follow the conclusion of Wenzel model that microstructures will make the intrinsic hydrophilic surface more hydrophilic. The intrinsic contact angle for surface with characteristic energy of 0.6 kcal/mol is 75.9°, and the simulation result shows that the apparent contact angle on the pillar surface is 98°. The same trend occurs for the surface with characteristic energy of 0.8 kcal/mol, the intrinsic contact angle is 62.3° and the apparent contact angle is 87.22°. Similar results were reported in previous studies [18,34]. It is noteworthy to consider the influence by the protrusion edge of a pillar on which the water droplet sits. The difference between the nanoscale and macroscale may cause that part of macroscopic conclusions are not appropriate at the nanoscale.

The dependence of contact angle on the pillar surface fraction, P, was also investigated. The characteristic energy was chosen to be 0.2379 kcal/mol. Rough surfaces with different number of pillars were constructed, as can be seen in Fig. 14. And Fig. 15 shows the time-average density contours of water droplet on different rough surfaces. With the value of P decreasing, the transition from the Cassie state to the Wenzel state arises, and this is because the smaller gaps limit the number of water molecules move down between pillars. If the water molecules move down to narrow gaps, the total energy of the system would be quite high and make the system unstable. From Fig. 16, we could draw the conclusion that the contact angle would increase with the decreasing pillar surface fraction within the scope of this paper. For the case P = 0.18, the wetting state is Cassie state, and the apparent contact angle is 149.45°, which is consistent to calculated value 151.83°. For the case P = 0.12, the wetting state becomes Wenzel state, and the apparent contact angle is 149.72°. The results for the two cases are quite similar.

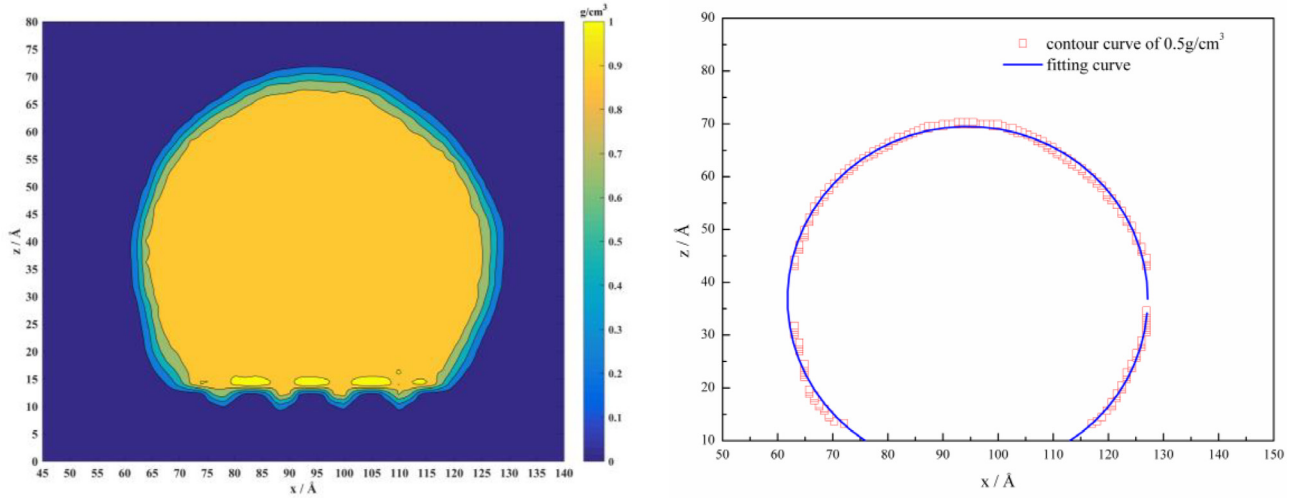

Fig. 9. Results of water droplet on the pillar surface whose P value is 0.4, ε_{solid} = 0.2379 kcal/mol.

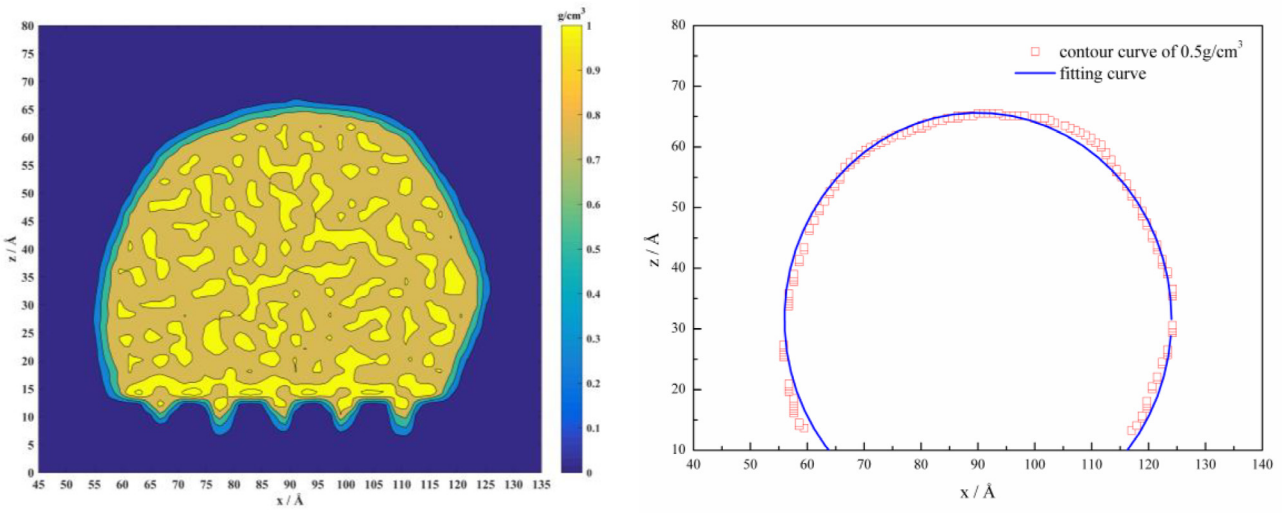

Fig. 10. Results of water droplet on the pillar surface whose P value is 0.4, ε_{solid1} = 0.4 kcal/mol.

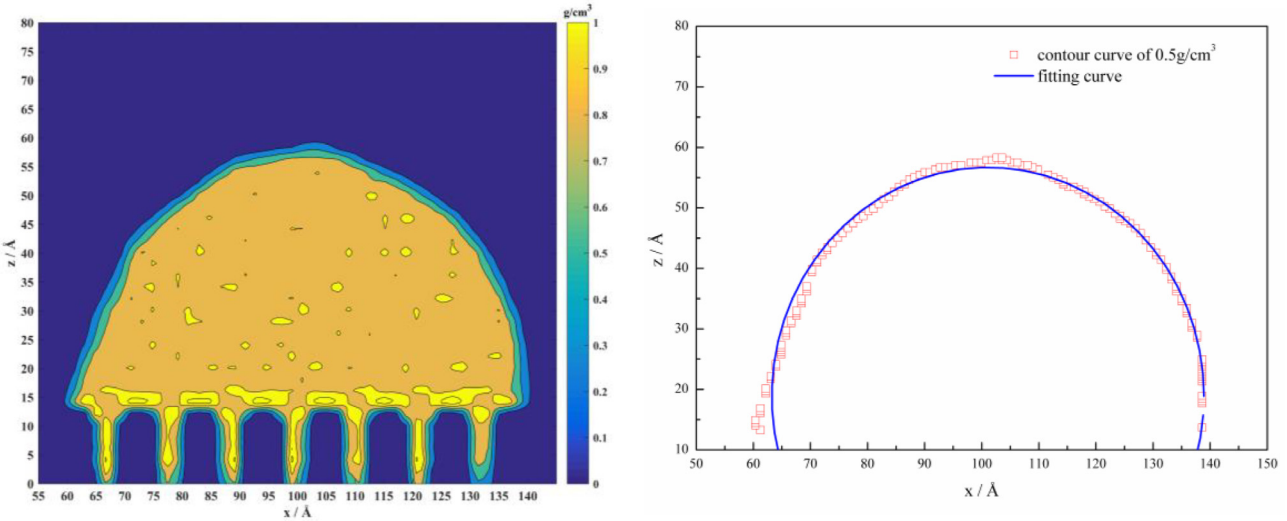

Fig. 11. Results of water droplet on the pillar surface whose P value is 0.4, ε_{solid2} = 0.6 kcal/mol.

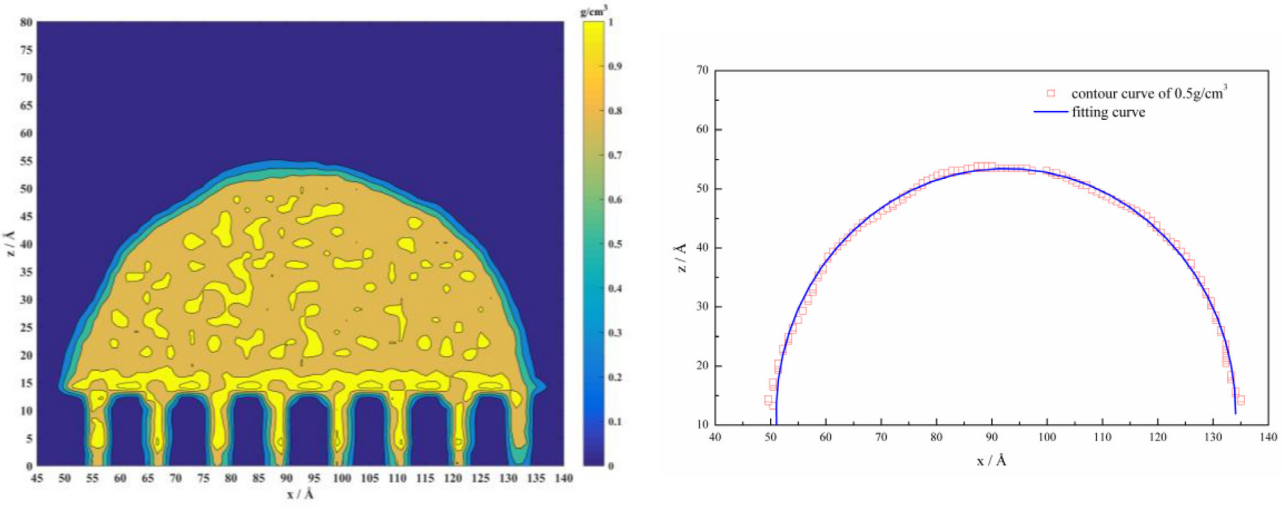

Fig. 12. Results of water droplet on the pillar surface whose P value is 0.4, ε_{solid3} = 0.8 kcal/mol.

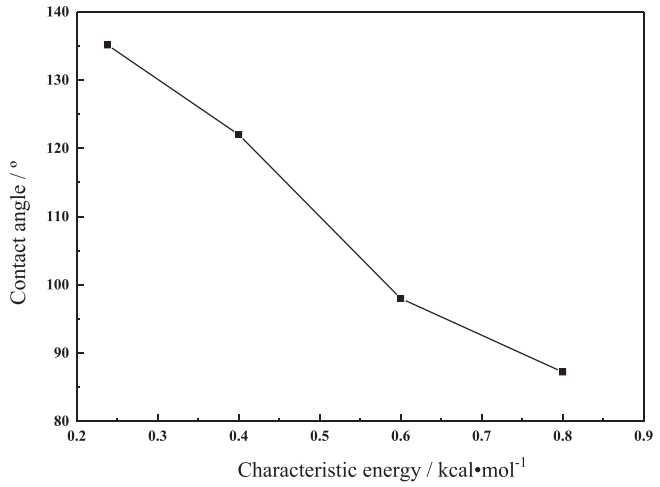

Fig. 13. Relationship between contact angle and characteristic energy, on the pillar surface.

3.4. Equivalent virtual surface analysis

To explain the effect of rough surfaces on contact angle, this paper proposes a method of equivalent virtual surface analysis. Only two-dimensional situations are considered in the present work, and it is enough to explain this problem. For the real ideal flat surface, the interactions between each pair of particles are considered in molecular dynamics simulation, as shown in Fig. 17, the red ones are the surface particles and the blue one is the liquid molecule. In this study, a virtual flat surface will be constructed and the virtual surface interacts with liquid molecules by generating forces on the atoms in the direction perpendicular to the virtual surface, as shown in Fig. 18. What's more the interactions between virtual surface and liquid molecules are equivalent to that between real ideal surface and liquid molecules.

The interaction between real ideal surface and liquid molecules is based on particle-particle interaction, that is each particle interacts with all particles within the cutoff distance, so the interaction direction may be random. In order to make a real ideal surface equivalent to a virtual surface, it is necessary to combine the interactions in different directions to obtain an equivalent interaction perpendicular to the virtual surface. Here, the interaction potential is considered as the equivalent. The particle-particle interaction potential is described by Eq. (1), and the Lennard-Jones potential function can be illustrated as Fig. 19. In Fig. 19, the characteristic energy of solid surface is chosen as 0.2379 kcal/mol, and the SPC/E water model only considers the interactions of oxygen atoms in water molecules with the wall-particles. According to the conclusions obtained in the previous section, small characteristic energy of solid surface represents weak interaction between solid particle and water which results in large contact angle, in contrast, large characteristic energy of solid surface represents strong interaction and lead to small contact angle. The strength of the interaction is reflected in the potential energy curve, which is the potential well depth. The deeper the potential well, the stronger the interaction.

Since the equivalent variable is interaction potential, the target is to draw the potential function curve between the virtual surface and oxygen atom. The independent variable of the potential function between oxygen atom and the virtual surface is the distance from the oxygen atom to the virtual surface, not the distance to the wall particles. In order to obtain the interaction between the oxygen atom and the virtual surface, it is necessary to calculate the potential energy of the oxygen atom at a different position from the real surface. For convenience of description, h is defined as the distance from oxygen atom to the surface. Even if the distance from oxygen atom to real surface is fixed, if the lateral position of the oxygen atom varies, the interaction potential energy will change. As shown in Fig. 20, the particle at position A1 and the particle at position B are at the same

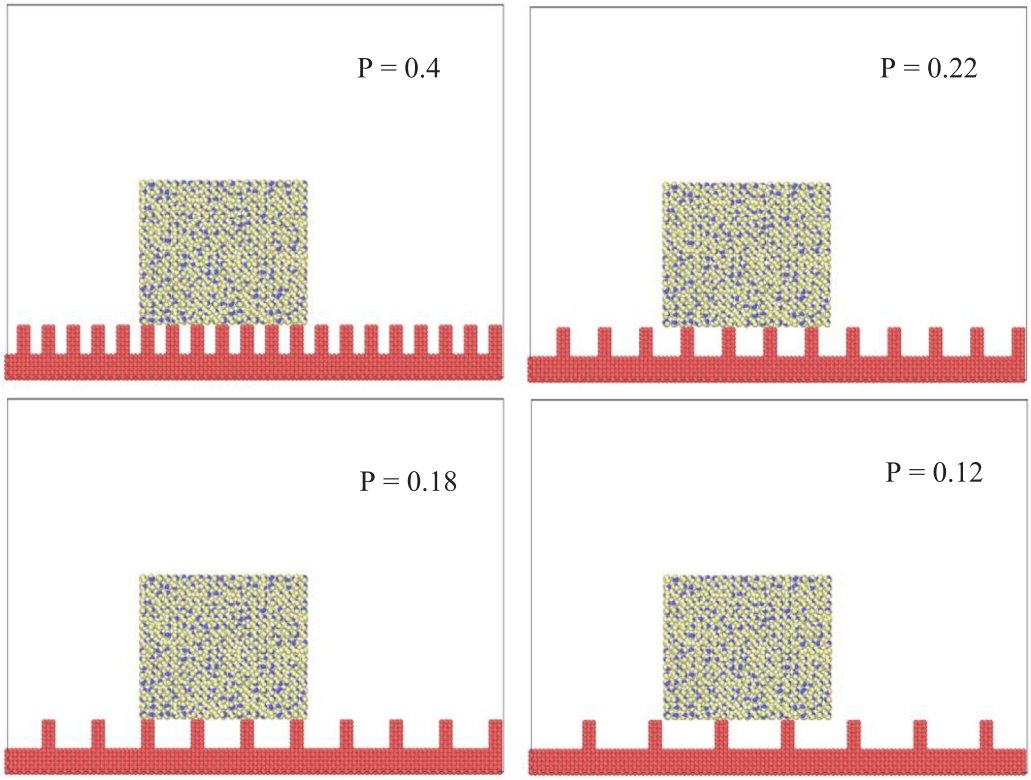

Fig. 14. Initial configurations of rough surfaces with different value of P, where P is defined as a geometric feature parameter to describe the roughness of the pillar surface which is the ratio of the pillar geometric projected area to the smooth surface.

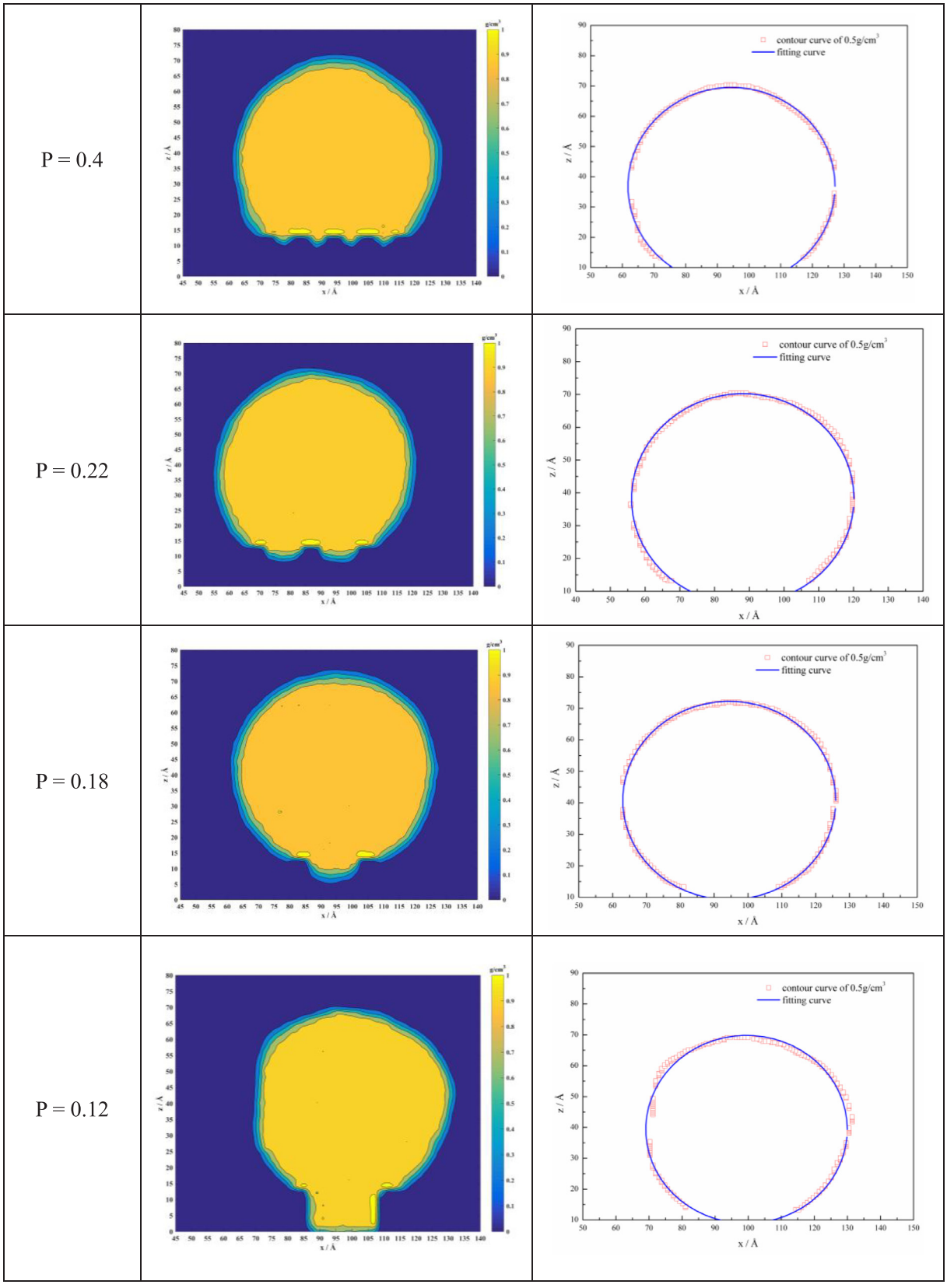

Fig. 15. Time-average density contours and the fitting-curves of water droplet on pillar surfaces with different value of P.

distance from the surface, but their interactions with the surface are different, whereas the position A1 and the position A2 are equivalent, the interactions of particles at these two positions with the surface are the same. Therefore, the interaction potential can be regarded as a periodic function that varies with x when the height h is fixed, and A1-A2 is a period. As shown in Fig. 21, the interaction potential between oxygen atom and the surface varies with the x position periodically at each height h. In order to obtain the equivalent interaction potential

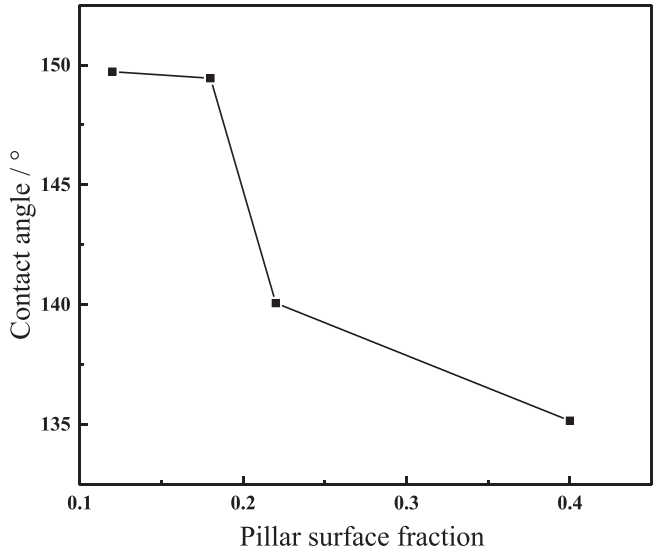

Fig. 16. Relationship between contact angle and pillar surface fraction.

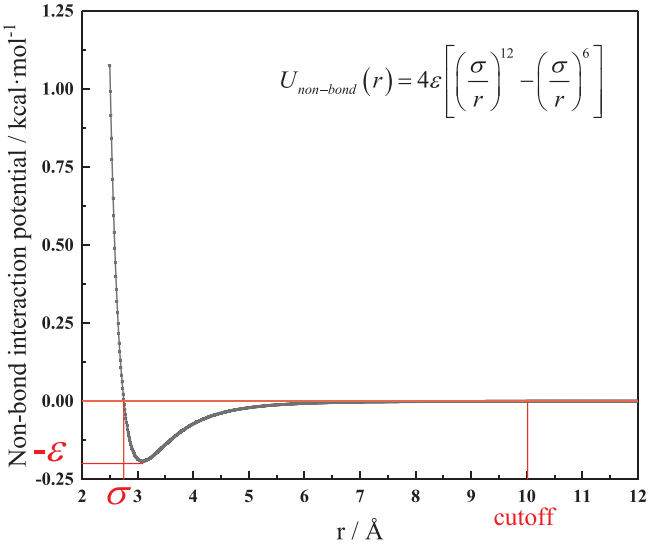

Fig. 19. Illustration of Lennard-Jones potential function.

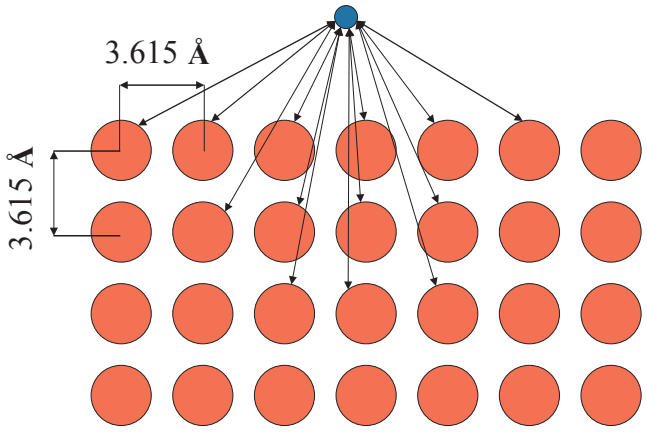

Fig. 17. Interaction between liquid molecule and real ideal surface.

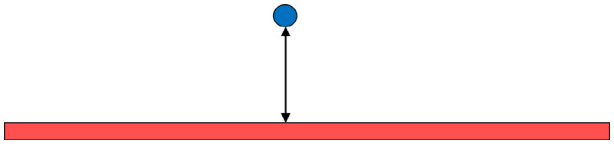

Fig. 18. Interaction between liquid molecule and equivalent virtual surface.

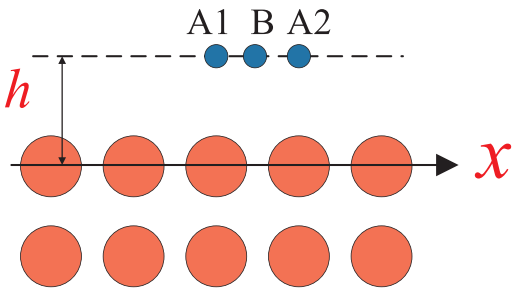

Fig. 20. Illustration of calculating the equivalent potential energy.

which is only related to the height h, the average potential energy at height h should be calculated. To this end, importance sampling method is applied. If an oxygen atom is placed at a height h from the surface randomly, the probability of appearing at different x coordinates is not the same, this probability is related to the distribution of interaction potential energy which are shown in Fig. 21. The average interaction potential energy at height h will be calculated through Eq. (6).

$$\langle U \rangle = \frac{\int \exp[-\beta U(x)] U(x) dx}{\int \exp[-\beta U(x)] dx} \tag{6}$$

The probability density at which oxygen atom appears at position x can be expressed as:

$$N(x) = \frac{exp[-\beta U(x)]}{\int exp[-\beta U(x)] dx} \tag{7}$$

In Eqs. (6) and (7), $U(x)$ means the distribution of interaction potential energy shown as Fig. 21, β can be calculated as Eq. (8), where k_B is the Boltzmann constant, and $T$is the temperature.

$$\beta = \frac{1}{k_B T} \tag{8}$$

By Eqs. (6)–(8), the average potential energy at height h can be obtained, and the red lines in Fig. 21 represent the average interaction potential energies for each h, that is, the equivalent interaction potential energy between oxygen atom and the equivalent virtual surface.

Therefore, the equivalent potential energy curve is shown in Fig. 22. In Fig. 22, the black curve with black square symbols represents the equivalent interaction potential curve for surface characteristic energy of 0.2379 kcal/mol, and the red curve with red circle symbols represents the equivalent interaction potential curve for surface characteristic energy of 0.8 kcal/mol. According to the above study, the contact angle of water droplets on a plane with a surface characteristic energy of 0.2379 kcal/mol is 110°, and the contact angle of water on a plane with a surface characteristic energy of 0.8 kcal/mol is 62.3°. The conclusion has been drawn that the contact angle decreases with increasing surface characteristic energy. Here, we propose an equivalent statement combining with equivalent potential energy, that is, the deeper the depth of the potential well of the equivalent potential energy curve, the smaller the contact angle. In Fig. 22, the depth of the potential well of red curve is deeper than the depth of the potential well of black curve, which indicates that the red curve corresponds to a smaller contact angle than the black curve. This confirms that the equivalent virtual surface analysis is available.

The equivalent virtual surface analysis is used to explain the wettability transition of pillar surface. The two-dimensional pillar surface shown in Fig. 23 is considered, and the surface characteristic energy is considered as 0.2379 kcal/mol. And the equivalent interaction potential

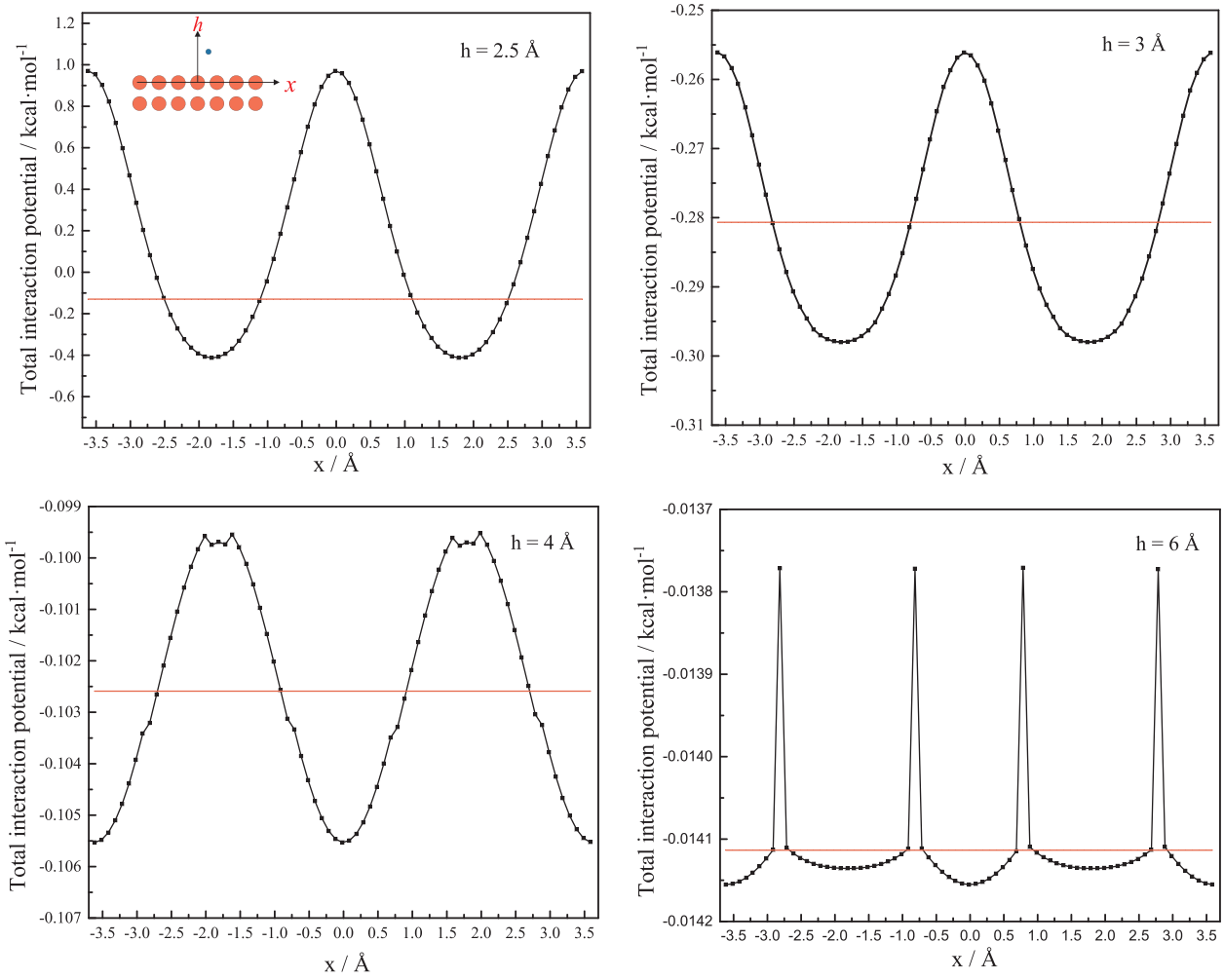

Fig. 21. The distribution of interaction potential energy when the h is fixed.

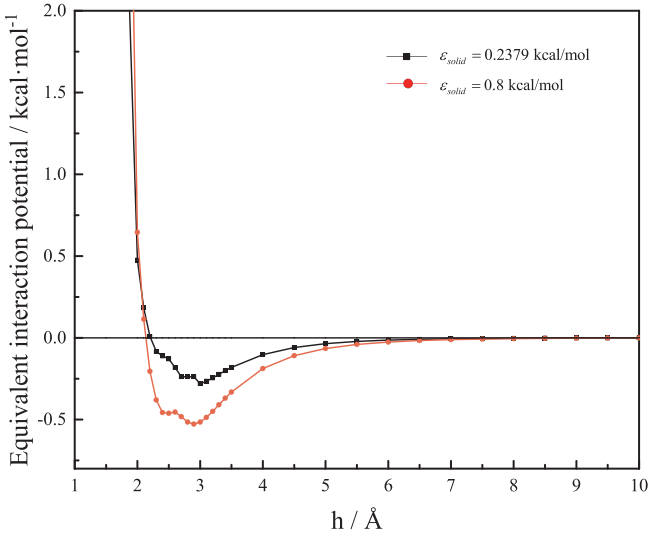

Fig. 22. Equivalent interaction potential curve.

curves shown in Fig. 24 indicate that the potential well depth of pillar surface is smaller than that of flat surface, which could explain why the surface nanostructure can change the surface wetting property and make the apparent contact angle lager than the intrinsic contact angle. It is worth noting that when the height his lower than about 2.5 Å, the

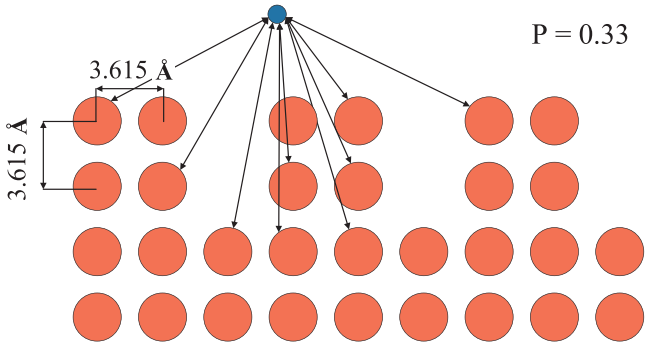

Fig. 23. Scheme of two-dimensional pillar surface of P = 0.33.

equivalent interaction potential does not increase with the decreasing of height. The reason is that the oxygen atom is more likely to appear above the gap when this height h is too low, because the interaction potential at that position is lower than that at other position which lead to higher probability of the event. And this cause the equivalent interaction potential lower according to the calculation process of the equivalent interaction potential energy described above. In addition, this explanation can be also confirmed in Fig. 15, it can be observed that even if the water droplet follows Cassie mode on the pillar surface, there will still be some water molecules extending into the gap between the pillars.

For the pillar surfaces with same fraction P = 0.33, if the

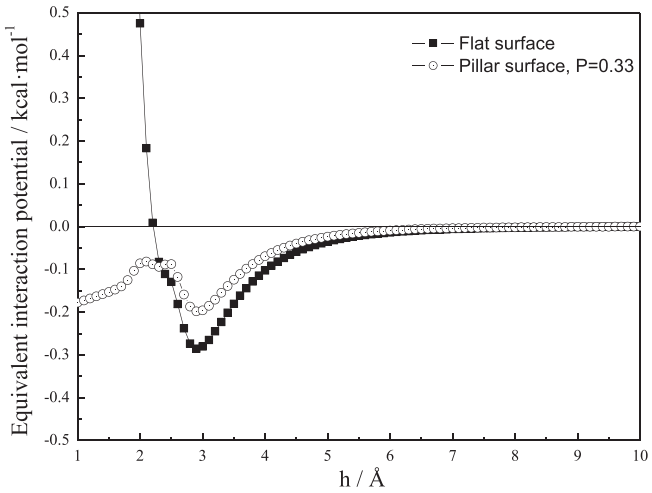

Fig. 24. Equivalent interaction potential curve of two-dimensional pillar surface of P = 0.33.

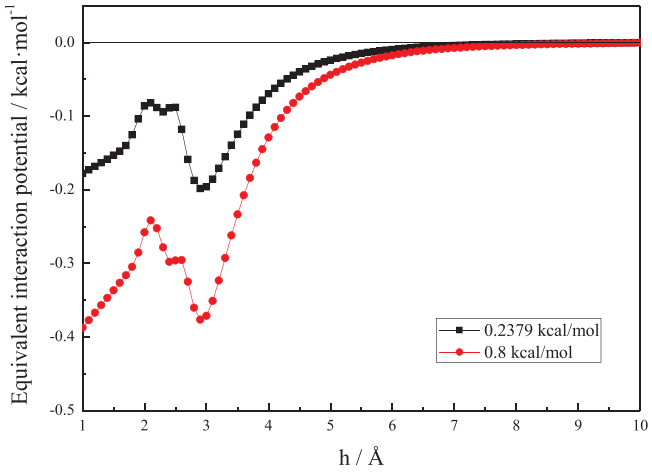

Fig. 25. Equivalent interaction potential curves of two-dimensional pillar surfaces of P = 0.33, with different surface characteristic energy.

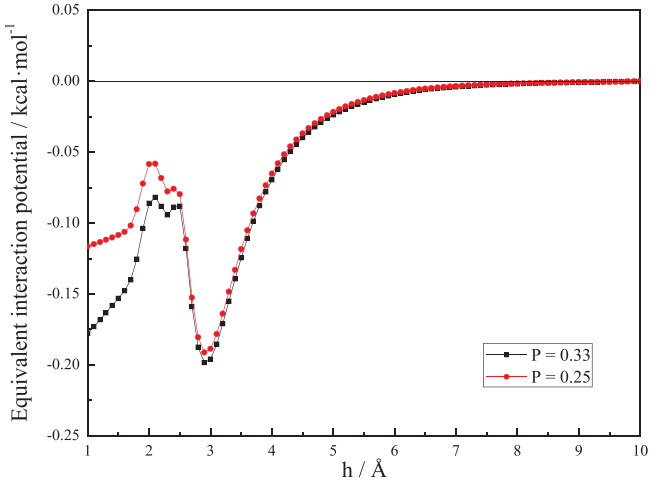

Fig. 26. Equivalent interaction potential curves of two-dimensional pillar surfaces of P = 0.33 and P = 0.25.

characteristic energy of the surface particles is changed, the equivalent interaction potential energy curve is shown in Fig. 25. From this figure, the contact angle of the surface characteristic energy of 0.8 kcal/mol is smaller than the surface with characteristic energy of 0.2379 kcal/mol, which can be interpreted that potential well of the equivalent interaction potential curve of the former is deeper.

As for the surfaces with same characteristic energy but different surface fraction P, from section 3.3, we have drawn the conclusion that the contact angle would increase with the decreasing pillar surface fraction. And in this section, the reason could be obtained from the Fig. 26 that the potential well of equivalent potential curve is slightly smaller for the surface with small P.

In summary, this section presents a method that can explain the changes in wettability of nanostructured surfaces, namely the equivalent virtual surface analysis.

4. Conclusions

This paper provides a molecular-level investigation on the mechanism of how the nanostructure changes surface wettability. To study the dependence of intrinsic contact angle on the surface characteristic energy, 2856 water molecules placed on flat surfaces with different characteristic energies were constructed. The results revealed that that the larger the surface characteristic energy, the smaller the contact angle. The contact angle decreased from 110° to 62.3° when the surface characteristic energy became larger from 0.2379 kcal/mol to 0.8 kcal/mol. In addition, the wetting behaviors on same nanostructure surface with different characteristic energies were simulated. The results showed that the nanostructured surface with low characteristic energy preferred to form Cassie state and the apparent contact angle obtained from simulation was consistent with that calculated by Cassie model. As for the nanostructured surface with high characteristic energy, it was easier to form Wenzel state, but the apparent contact angle obtained from simulation deviate greatly from the Wenzel model value. It seemed that Wenzel model was not appropriate at nanoscale. What's more, the effect of different nanostructures on apparent contact angle was investigated. Nanostructured pillar surfaces with different pillar surface fractions were constructed. The static contact angle would increase with the decrease of pillar surface fraction. Finally, this paper proposed an equivalent virtual surface analysis to state the relationship between contact angle and equivalent interaction potential. The method determines the change in contact angle by the depth of potential well. The deeper the potential well, the smaller the contact angle. The potential well depth of nanostructured surface was smaller than that of flat surface, which indicated that nanostructured surface would be more hydrophobic.

Acknowledgement

This work has been supported by the National Natural Science Foundation of China (Grant number 51876161).

References

[1] W. Barthlott, C. Neinhuis, Purity of the sacred lotus, or escape from contamination in biological surfaces, Planta 202 (1) (1997) 1–8.
[2] X.F. Gao, L. Jiang, Water-repellent legs of water striders, Nature 432 (7013) (2004) 36–36.
[3] R. Karmouch, G.G. Ross, Experimental study on the evolution of contact angles with temperature near the freezing point, J. Phys. Chem. C 114 (9) (2010) 4063–4066.
[4] Y.G. Zhao, H. Zhang, W. Wang, C. Yang, Wetting transition of sessile and condensate droplets on copper-based superhydrophobic surfaces, Int. J. Heat Mass Transf. 127 (2018) 280–288.
[5] T. Werder, J.H. Walther, R.L. Jaffe, T. Halicioglu, F. Noca, P. Koumoutsakos, Molecular dynamics simulation of contact angles of water droplets in carbon nanotubes, Nano Lett. 1 (12) (2001) 697–702.
[6] J.T. Hirvi, T.A. Pakkanen, Molecular dynamics simulations of water droplets on polymer surfaces, J. Chem. Phys. 125 (14) (2006) 11.
[7] B. Ohler, W. Langel, Molecular dynamics simulations on the interface between titanium dioxide and water droplets: a new model for the contact angle, J. Phys. Chem. C 113 (23) (2009) 10189–10197.
[8] R.C. Dutta, S. Khan, J.K. Singh, Wetting transition of water on graphite and boron-nitride surfaces: a molecular dynamics study, Fluid Phase Equilib. 302 (1–2) (2011) 310–315.

[9] R. Burt, G. Birkett, M. Salanne, X.S. Zhao, Molecular dynamics simulations of the influence of drop size and surface potential on the contact angle of ionic-liquid droplets, J. Phys. Chem. C 120 (28) (2016) 15244–15250.
[10] C.T. Nguyen, B. Kim, Stress and surface tension analyses of water on graphene-coated copper surfaces, Int. J. Precis. Eng. Manuf. 17 (4) (2016) 503–510.
[11] C. Chen, B. Dong, N. Zhang, W.Z. Li, Y.C. Song, Pressure and temperature dependence of contact angles for co2/water/silica systems predicted by molecular dynamics simulations, Energy Fuels 30 (6) (2016) 5027–5034.
[12] C. Chen, J.M. Wan, W.Z. Li, Y.C. Song, Water contact angles on quartz surfaces under supercritical CO_2 sequestration conditions: experimental and molecular dynamics simulation studies, Int. J. Greenh. Gas Control 42 (2015) 655–665.
[13] C. Zhang, Z. Liu, P. Deng, Contact angle of soil minerals: a molecular dynamics study, Comput. Geotech. 75 (2016) 48–56.
[14] T.S. Wong, C.M. Ho, Dependence of macroscopic wetting on nanoscopic surface textures, Langmuir 25 (22) (2009) 12851–12854.
[15] R.N. Wenzel, Resistance of solid surfaces to wetting by water, Ind. Eng. Chem. 28 (1936) 988–994.
[16] C.W. Extrand, Model for contact angles and hysteresis on rough and ultraphobic surfaces, Langmuir 18 (21) (2002) 7991–7999.
[17] S. Chen, J.D. Wang, D.R. Chen, States of a water droplet on nanostructured surfaces, J. Phys. Chem. C 118 (32) (2014) 18529–18536.
[18] D. Niu, G.H. Tang, Static and dynamic behavior of water droplet on solid surfaces with pillar-type nanostructures from molecular dynamics simulation, Int. J. Heat Mass Transf. 79 (2014) 647–654.
[19] S. Chen, J.D. Wang, T.B. Ma, D.R. Chen, Molecular dynamics simulations of wetting behavior of water droplets on polytetrafluorethylene surfaces, J. Chem. Phys. 140 (11) (2014) 8.
[20] C.D. Daub, D. Bratko, K. Leung, A. Luzar, Electrowetting at the nanoscale, J. Phys. Chem. C 111 (2) (2007) 505–509.
[21] C.D. Daub, D. Bratko, A. Luzar, Electric control of wetting by salty nanodrops: molecular dynamics simulations, J. Phys. Chem. C 115 (45) (2011) 22393–22399.
[22] F.H. Song, L. Ma, J. Fan, Q.C. Chen, L.H. Zhang, B.Q. Li, Wetting behaviors of a nano-droplet on a rough solid substrate under perpendicular electric field, Nanomaterials 8 (5) (2018) 12.
[23] B. Shi, V.K. Dhir, Molecular dynamics simulation of the contact angle of liquids on solid surfaces, J. Chem. Phys. 130 (3) (2009) 5.
[24] K. Fei, C.P. Chiu, C.W. Hong, Molecular dynamics prediction of nanofluidic contact angle offset by an AFM, Microfluid. Nanofluid. 4 (4) (2008) 321–330.
[25] S.D. Hong, M.Y. Ha, S. Balachandar, Static and dynamic contact angles of water droplet on a solid surface using molecular dynamics simulation, J. Colloid Interface Sci. 339 (1) (2009) 187–195.
[26] T. Koishi, K. Yasuoka, S. Fujikawa, X.C. Zeng, Measurement of contact-angle hysteresis for droplets on nanopillared surface and in the cassie and wenzel states: a molecular dynamics simulation study, ACS Nano 5 (9) (2011) 6834–6842.
[27] E. Bertrand, T.D. Blake, J. De Coninck, Influence of solid-liquid interactions on dynamic wetting: a molecular dynamics study, J. Phys.-Condes. Matter 21 (46) (2009) 14.
[28] S. Plimpton, Fast parallel algorithms for short-range molecular-dynamics, J. Comput. Phys. 117 (1) (1995) 1–19.
[29] H.J.C. Berendsen, J.R. Grigera, T.P. Straatsma, The missing term in effective pair potentials, J. Phys. Chem. 91 (24) (1987) 6269–6271.
[30] X. Wang, D.W. Jing, Determination of thermal conductivity of interfacial layer in nanofluids by equilibrium molecular dynamics simulation, Int. J. Heat Mass Transf. 128 (2019) 199–207.
[31] J.P. Ryckaert, G. Ciccotti, H.J.C. Berendsen, Numerical integration of the cartesian equations of motion of a system with constraints: molecular dynamics of n-alkanes, J. Comput. Phys. 23 (3) (1977) 327–341.
[32] C.M. Tenney, R.T. Cygan, Molecular simulation of carbon dioxide, brine, and clay mineral interactions and determination of contact angles, Environ. Sci. Technol. 48 (3) (2014) 2035–2042.
[33] Z.J. Cheng, M. Du, H. Lai, N.Q. Zhang, K.N. Sun, Super-hydrophobic copper surface with controlled adhesion prepared via ammonia corrosion, Chem. J. Chin. Univ.-Chin. 34 (3) (2013) 606–609.
[34] W.J. Jeong, M.Y. Ha, H.S. Yoon, M. Ambrosia, Dynamic behavior of water droplets on solid surfaces with pillar-type nanostructures, Langmuir 28 (12) (2012) 5360–5371.